MRE-Binding Transcription Factor-1: Weak Zinc-Binding Finger Domains 5 and 6 Modulate the Structure, Affinity, and Specificity of the Metal-Response Element Complex†

Xiaohua Chen, Meihua Chu, and David P. Giedroc*

Department of Biochemistry and Biophysics, Center for Macromolecular Design, Texas A&M University, College Station, Texas 77843-2128

Received June 8, 1999; Revised Manuscript Received July 27, 1999

ABSTRACT: MRE-binding transcription factor-1 (MTF-1) contains six Cys_2-His_2 zinc finger sequences, and it has been suggested that the zinc finger domain itself may function as a zinc sensor in zinc-activated expression of metallothioneins (MTs). Previous work has shown that a subset (≈3−4) of the zinc fingers in MTF-zf play a structural role in folding and high-affinity metal-response element (MREd) binding, while one or more other fingers have properties consistent with a metalloregulatory role (weak zinc binding affinity in the absence of DNA). We show here that zinc fingers 5 and 6 correspond to the weak zinc-binding fingers in MTF-zf. Limited trypsinolysis of a Zn_6-MTF-zf:MREd complex gives rise to a highly protease-resistant core fragment corresponding to amino acids 137−260 or N-terminal zinc fingers 1−4 of MTF-zf. Characterization of a collection of broken-finger (His → Asn) and missing-finger mutants of MTF-zf reveals that deletion of zinc fingers 5 and 6 to create MTF-zf14 attenuates MREd binding affinity (≈20-fold), while deletion of fingers 4−6 (MTF-zf13) results in a further 20-fold reduction of binding affinity with a nearly complete loss of specificity. Circular dichroism studies reveal that the binding of MTF-zf to the MREd induces a dramatic alteration of the structure of the MREd from a B-form to a double-helical conformation with A-like features. Formation of stoichiometric complexes with MTF-zf14, H279N (Δzf5) MTF-zf, and MTF-zf13 induces comparatively less A-like structure. Steady-state fluorescence resonance energy transfer (FRET) spectroscopy has been used to globally define the orientation of the multifinger MTF-zf on the MREd. These experiments suggest that fingers 1−4 are oriented on the highly conserved TGCRCnC side of the MREd with fingers 5−6 bound at or near the gGCCc sequence. These findings are consistent with a model in which the N-terminal zinc fingers in MTF-zf are required for high affinity and specific binding to the consensus TGCRCnC core in a way which is subjected to structural and allosteric modulation by the weak zinc-binding C-terminal zinc fingers.

All organisms have evolved regulatory mechanisms to effect heavy metal ion homeostasis, defined as maintaining the concentration of essential metal ions, such as zinc, copper, and iron, at levels that are optimal to cellular metabolism, coupled with the expulsion of toxic metals, e.g., mercury, cadmium, and arsenates, which play no biological role (*3*). Distinct control mechanisms for the homeostasis of essential metal ions are known to operate depending on whether the cell senses that there is limiting or excess free metal concentrations present intracellularly. In general, under metal-deficient conditions, the transcription of genes which encode for membrane uptake and intracellular transport proteins is activated which enables the cell to efficiently scavenge metal from the environment and utilize it. Under conditions of excess metal, the expression of genes encoding specific metal export pumps (e.g., P-type ATPases which function as membrane transporters) or highly specific, intracellular metal chelators such as metallothioneins in cyanobacteria and vertebrate cells and phytochelatins in plants, which sequester metals, are two common regulatory mechanisms used to maintain the concentration of an essential metal ion in the acceptable range.

With the prominent exception of iron regulation in mammalian cells (*4*), nearly all of the cell-type-specific regulatory mechanisms associated with the control of gene expression in metal homeostasis operate transcriptionally (*3*). In many cases, the transcription factors which bind specifically to cis-acting DNA elements positively or negatively regulate the expression of these genes and are allosterically activated or inhibited by the direct binding of metals to the transcription factor itself (*5, 6*). These transcription factors are therefore metalloregulatory molecules, which sense *and* transduce the biological response to a metal-deficient or metal-excess condition. The paradigm for this type of regulatory control remains *Escherichia coli* MerR, which is a transcriptional repressor of the expression mercuric reductase in the absence of toxic mercury but becomes a positive activator in the presence of mercury (*7*). The specificity of these kinds of regulatory transcriptional switches is hypothesized to lie largely at the level of coordination chemistry. In eubacteria, at least three families of evolutionarily conserved metalloregulatory transcription factors are now

† This work was supported by NIH Grant GM42569 and the Robert A. Welch Foundation (Grant A-1295).

* To whom correspondence should be addressed. Telephone: 409-845-4231. Fax: 409-862-4718. E-mail: giedroc@tamu.edu.

10.1021/bi9913000 CCC: $18.00
Published on Web 09/11/1999

known to exist. These are the ArsR family (*8*) and two families of iron-dependent negative repressor proteins, the Fur and Fur-like proteins from gram-negative bacteria (*9, 10*) and DtxR-related repressors from Gram-positive bacteria (*11*); in no case has it been quantitatively determined, with the exception of MerR (*12*), the extent to which these regulatory factors are specific for one type of metal ion over another.

Zinc plays essential and ubiquitous catalytic and structural roles in all of biology, present at the active sites of many hydrolytic enzymes and as an integral tertiary structural element in many proteins, most prominently exemplified by zinc finger proteins (*13*−*15*). Zinc-specific metalloregulation has been documented to occur in all organisms in which it has been sought, including mammalian cells (*16*), plants (*17*), yeast (*18*), and bacteria (*19*−*21*). Zinc metalloregulatory transcription factors have been identified, cloned, and partially characterized from a variety of cyanobacterial (*22, 23*) and other eubacterial organisms which mediate the response of cells to both zinc-deficient and zinc-replete conditions (*10, 19*). *E. coli* (*19*) and *Bacillus subtilis* (*10*) Zur are evolutionarily related to *E. coli* ferric uptake repressor (Fur) (*24*), which regulates the iron-dependent repression of iron-uptake systems, and appear to be zinc-activated repressors of high-affinity zinc-uptake pathways in these cells. The cyanobacteria *Synechococcus* (*25*) and *Synechocystis* (*23*) encode homologous repressor molecules which regulate the expression of metallothionein and an apparently zinc-specific export pump, respectively, the expression of which is derepressed under conditions of zinc excess. In *Saccharomyces cerevisiae*, Zap1p is a zinc-regulated transcription factor which actives the expression of both high- and low-affinity zinc uptake systems under zinc-limiting conditions (*26*). In mammalian cells, zinc homeostasis appears to be largely maintained by the zinc-dependent transcriptional regulation of metallothionein (MT) genes (*27*), which requires the interaction of metal-response element (MRE)-binding transcription factor-1 (MTF-1)[1] (*28, 29*) with metal-response elements (MREs) (*30*) situated upstream of zinc-inducible genes.

Both *S. cerevisiae* Zap1p (*26*) and MTF-1 (*16*) contain multiple, canonical TFIIIA-like Cys_2-His_2 zinc fingers (*31*), one or more of which have been hypothesized to play a direct role in zinc metalloregulation (*16, 32*). However, their regulatory mechanisms have clearly diverged since Zap1p is a transcriptional activator, the activity of which is induced under zinc-limiting conditions, while MTF-1 is a transcription activator whose activity is induced under conditions of zinc excess. MTF-1 is a constitutively expressed protein in mouse and human cells of ≈80 kD that contains six Cys_2-His_2 zinc fingers and multiple domains for transcriptional activation (*28*). The disruption of both alleles of the MTF-1 gene in mouse embryonic stem cells by homologous recombination showed that the resulting null mutant cell line fails to produce detectable amounts of MTF-1 (*29*). Moreover, due to the loss of MTF-1, the endogenous metallothionein I and II genes are silent, indicating that MTF-1 is essential for basal and heavy metal-induced metallothionein gene expression (*29*). A recent report shows that the MTF-1 and MREs are required for regulation of glutathione biosynthetic genes, linking zinc homeostasis with the maintenance of an appropriate redox potential inside cells (*33*) consistent with previous findings that oxidative stress also activates MTF-1 MRE-binding activity (*34*). Although other toxic heavy metals, including cadmium, are also know to induce the expression of metallothioneins (MT-I) in vertebrate cells (*35*), it now seems clear that this induction is mechanistically distinct from zinc-dependent induction and does not require MTF-1 (*36*−*38*).

Several reports suggest that MTF-1 itself is a zinc sensor which exhibits increased DNA binding activity upon zinc treatment in vivo and in vitro (*29, 36*). In previous work from our laboratory, we reported that the Cys_2-His_2 zinc fingers of a zinc finger domain fragment of MTF-1 (denoted MTF-zf) are physically and functionally inequivalent (*2*). A subset (≈3−4) of zinc fingers plays a structural role in folding and high-affinity binding to zinc, while one or more additional fingers have biochemical properties potentially consistent with a metalloregulatory role. Here, we show that the high-affinity zinc binding fingers of MTF-zf correspond to the N-terminal fingers 1−4, and when bound to the MRE, an N-terminal fragment of MTF-zf encompassing all of zinc fingers 1−4 is strongly protected from proteolysis; this suggests that fingers 1−4 and 5 and 6 make distinct interactions with the MRE. Fluorescence resonance energy transfer experiments have been used to define the overall orientation of MTF-zf on the MRE. Previous studies showed that zinc occupancy of the weak binding C-terminal fingers does not detectably alter the affinity of complex formation provided the Cys are in their reduced state (*2*). Here we make the striking finding that deletion or mutation of fingers 5 and 6 results in a loss of MREd binding affinity and specificity, each of which is strongly correlated to a pronounced conformational change in the MRE, from a typical B-form structure to a conformation with features like A-form polynucleotides. This suggests the possibility that allosteric metalloregulation in this system may lie in part at the level of DNA conformational changes.

MATERIALS AND METHODS

Construction of pT7MTF-zf14, pT7MTF-zf13, pT7MTF-zf46, pT7MTF-H279N, and pT7MTF-H309N. Bacterial expression plasmids, pT7MTF-zf14 (expressing residues 137−259), pT7MTF-zf13 (expressing residues 137−229), and pT7MTF-zf46 (expressing residues 226−320) of human MTF-1, were constructed by amplifying a DNA fragment via the polymerase chain reaction using the cDNA plasmid pChMTF-1 (obtained from Dr. W. Schaffner, University of Zürich) as the template. The PCR primers incorporated *Nco*I and *Bgl*II restriction endonuclease sites, to permit subcloning of the crude PCR product directly into *Nco*I/*Bam*HI-restricted pET-3d. The 3′ PCR primer also directs substitution of the C-terminal Phe^{259} (MTF-zf14), Phe^{229} (MTF-zf13), and Tyr^{320} (MTF-zf46) of MTF-1 with Trp.

A PCR-based mutagenesis procedure was used to substitute the first conserved histidine of MTF-zf zinc finger 5 and 6 with a nonliganding asparagine (*39*) to create broken-finger (*40*) mutants H279N and H309N MTF-zf, respectively. pChMTF-1 was used as template for PCR amplification. For each mutation, two sets of overlapping primers were used to generate two overlapping PCR fragments. One fragment

[1] Abbreviations: DTNB, 5,5′-dithiobis(2-nitrobenzoic acid); MOPS, 3-(*N*-morpholino)propanesulfonic acid; MRE, metal-response element; MT, metallothionein; MTF-1, MRE-binding transcription factor-1.

was amplified with a primer which is complementary to 5′ end of the MTF-zf gene (bearing an *Nco*I site, 5′-TTA TGA *CCA TGG* TAA AGC GGT ACC AAT G-3′) and corresponding reverse primer (5′-CGA ACG TTA GTT TTA AGG-3′ for MTF-H279N and 5′-AGA TCT TTA CTA CCA TGA GTG TCC TTT GTT ATC ATG ACC TTT CAT GTT ACT TTT G-3′ for MTF-H309N). The other fragment was amplified using the appropriate forward primer (e.g., 5′-CCT TAA AAC TAA CGT TCG-3′ for MTF-H279N) and a reverse primer complementary to the 3′ end of the MTF-zf gene (containing a *Bgl*II site, 5′-*AGA TCT* TTA CTA CCA TGA GTG TCC TTT GTT ATC ATG ACC-3′). The two fragments were amplified separately and then mixed and used to make a full-length PCR fragment using 5′ end and 3′ end primers with the CAC codon encoding the appropriate histidine residue changed to AAC codon encoding asparagine. The full-length PCR products were the blunt-ended with Klenow treatment, cloned into the *Sma*I site of pKAN2, and screened on X-gal-containing agar plates (12 μg/mL kanamycin). White colonies were chosen for amplification, and miniprep DNA was digested with *Nco*I and *Bgl*II to identify plasmids containing inserts. Subsequently, the *Nco*I-*Bgl*II fragment in each case was subcloned into the T7 expression vector, pET-3d, restricted with *Nco*I and *Bam*HI. The integrity of all recombinant pET expression vectors was verified by sequencing using Sequenase (USB).

Purification of MTF-zf14, MTF-zf13, MTF-zf46, H279N-MTF-zf, and H309N-MTF-zf. All MTF-zf protein mutants were expressed in *E. coli* BL21(DE3) and purified using nondenaturing conditions essentially as described previously for MTF-zf (*2*). Various aliquots of this material were subjected to exhaustive dialysis in an anaerobic glovebox (Vacuum-Atmospheres, Inc.) against metal-free buffer at pH 7.0, involving 4 changes over 8 h, and the zinc content and number of reduced cysteines were determined by flame atomic absorption and DTNB reactivity anaerobically, respectively, using $\epsilon_{280} = 14\,600$ M^{-1} cm^{-1} for MTF-zf14, $\epsilon_{280} = 12\,800$ M^{-1} cm^{-1} for MTF-zf13, $\epsilon_{280} = 9\,200$ M^{-1} cm^{-1} for MTF-zf46, $\epsilon_{280} = 16\,400$ M^{-1} cm^{-1} for H279N-MTF-zf and H309N-MTF-zf, essentially as described (*2*). Analytical data show that MTF-zf14 contained 8 reduced cysteines, while 6 reduced cysteines were found for MTF-zf13 and MTF-zf46, with ≈12 reduced cysteines for H279N and H309N MTF-zfs, consistent with predictions from the amino acid sequence. The Zn(II) contents of these proteins were 3.0 (3 expected), 3.2 (4), 2.7 (3), 4.9 (*3*−*5*), and 3.6 (*3*−*5*) g at mol^{-1} for MTF-zf13, MTF-zf14, MTF-zf46, H279N-MTF-zf, and H309N-MTF-zf proteins, respectively.

Preparation of Coumarin-Labeled DNAs. Crude oligonucleotides were obtained from Operon Technologies, purified by denaturing PAGE, modified with 7-(diethylamino)-coumarin-3-carboxylic acid, succinimidyl ester (Molecular Probes), purified by C4 reverse phase HPLC and desalted by C18 cartridge elution exactly as described previously (*2*). To prepare the duplexes shown in Figure 2, the purified coumarin-labeled oligonucleotides were annealed to their complementary unlabeled strands (1.05:1 unlabeled to labeled strand) at 95 °C for 5 min in 10 mM Tris-HCl, pH 7.5, followed by slow cooling at room temperature. Duplexes used in this way were used without further purification.

Fluorescence Measurements. All fluorescence polarization binding experiments were carried out with an SLM 8000 or

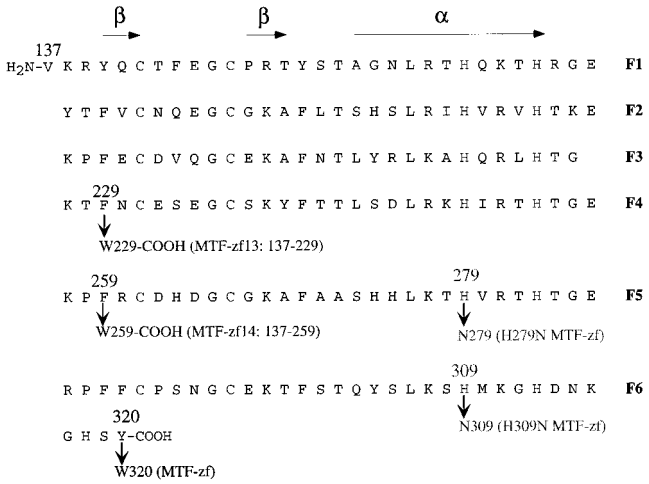

FIGURE 1: Amino acid sequences of MTF-zf, missing-finger mutants MTF-zf14 and MTF-zf13, and broken-finger mutants H279N MTF-zf (Δzf5) and H309N MTF-zf (Δzf6). Missing-finger mutant MTF-zf46 corresponds to residues 226−320 with the Trp^{320} substitution.

Consensus 5′-ctn**TGCR**CnCg**GCCc**

MREd1* 5′-GAGCTC**TGCA**CTCC**GCCC**GAAAA
LCTCGAGACGTGAGGCGGGCTTTT-5′

MREd2* 5′-GAGCTC**TGCA**CTCC**GCCC**GAAAA
CTCGAGACGTGAGGCGGGCTTTT**L**-5′

MUT1 5′-GAGCTC**TGCA**CTCCG**GAG**G**T**AAA
CTCGAGACGTGAGGCCTCCATTT**L**-5′

MUT2 5′-GAGCTC**CCATT**T**A**C**GCCC**GAAAA
CTCGAGGGTAAATGCGGGCTTTT**L**-5′

FIGURE 2: Sequences of the DNA duplexes used in this study. The L represents the coumarin moiety.

4800 spectrofluorometer operating in the steady-state mode fitted with Glan-Thompson polarizers used in the L format exactly as described previously (*2*). Nonlinear least-squares fits to these binding isotherms to extract K_{app} and $r_{complex}$ were carried out assuming a 1:1 binding stoichiometry (consistent with stoichiometric titrations) (*2*) and a linear change in r_{obs} with fractional saturation of the DNA. For reasons described previously (*2*), the small change in the quantum yield of the oligonucleotide observed in some cases upon protein binding was neglected and raw r_{obs} vs $[MTF\text{-}zf]_{total}$ isotherms were fit directly.

For experiments in which binding of MTF-zf and MTF-zf14 to MREd was monitored by fluorescence resonance energy transfer (FRET) from the C-terminal tryptophan donor to the coumarin acceptor, full sensitized emission spectra were collected for the appropriate coumarin-labeled MREd (MREd:1* or MREd:2*; see Figure 2) as a function of added MTF-zf or MTF-zf14 upon excitation at 295 nm (4 nm slit) (*41*). Corrected coumarin emission spectra (scanned from either 300−550 nm or 425−525 nm) were obtained by first subtracting the buffer-only emission spectrum, followed by subtracting the contribution of Trp fluorescence; the resulting spectrum was then corrected for dilution and inner filter

effects due to protein absorption. The efficiency of FRET when the coumarin−labeled DNA is saturated with bound protein (E) is related to the fluorescence intensity (F; λ_{ex} = 295 nm)of the coumarin acceptor in the presence (F_{ad}) and absence (F_a) of the donor quantified at λ_2 = 478 nm, the quantum yield of the acceptor in the presence (Q_{ad}) and absence (Q_a) of donor when only the acceptor is excited (λ_{ex} = 430 nm), and the absorbance of the acceptor ($\epsilon_{ad}C_{AT}$) and of the donor ($\epsilon_{da}.C_{DT}$) at the excitation wavelength (λ_1 = 295 nm), according to (*42*) the following:

$$E = [\epsilon_{ad}(\lambda_1)C_{AT}/\epsilon_{da}(\lambda_1)C_{DT}][((Q_a/Q_{ad})(F_{ad}(\lambda_2)/F_a(\lambda_2)) - 1] \quad (1)$$

ϵ_{ad} was calculated from a difference molar absorption spectrum obtained from subtraction of an unlabeled MREd spectrum from the coumarin-labeled DNA spectrum to obtain the contribution due only to the acceptor dye. For MREd: 1*, ϵ_{da} = 18 950 M^{-1} cm^{-1}, while, for the MREd:2* oligonucleotide, ϵ_{da} = 11 600 M^{-1} cm^{-1}. ϵ_{ad} for MTF-zf and MTF-zf14 was calculated from a molar absorptivity spectrum of each protein used to obtain the quantum yields (Q_d) of the Trp donor in each case. For MTF-zf, ϵ_{da} = 3524 M^{-1} cm^{-1}; for MTF-zf14, ϵ_{da} = 3084 M^{-1} cm^{-1}. E, in turn is related to R, the donor−acceptor distance, and R_o, the critical Förster distance where energy transfer is 50% efficient, according to

$$R = R_o(E^{-1} - 1)^{1/6} \quad (2)$$

where

$$R_o = 9790(\kappa^2 n^{-4} Q_d J) \quad (3)$$

where κ^2 is the orientation factor, n is the refractive index (taken as 1.4), Q_d is the quantum yield of the donor, and J is the spectral overlap interval (in units of M^{-1} cm^3), calculated as previously described (*43*).

Circular Dichroism Spectroscopy. Unless otherwise indicated, far-UV-CD spectra were collected on an Aviv 62DS spectropolarimeter operating at 25.0 ± 0.1 °C in a 1-mm rectangular cell with an MTF-zf concentration of 6−7 μM in 6 mM sodium phosphate, pH 7.0, and 0.20 M NaF. Typical acquisition parameters were 2 s time constant, 1 nm bandwidth, and 4−10 replicates. In the MREd-containing samples, the DNA concentration was 7 μM with sufficient protein present to ensure saturation of the DNA (1−5 molar equiv), based on K_{app} determined from fluorescence anisotropy titrations. All spectra were baseline corrected by subtraction of an averaged scan derived from the buffer alone and are presented in units of mean residue (amino acid or nucleotide as appropriate) ellipticity $[\theta]_{MRE}$ (deg cm^2 $dmol^{-1}$).

Limited Trypsinolysis Experiments. One microliter of 1 μg/μL trypsin was added to a 35 μM MTF-zf (6 Zn^{2+} or 3 Zn^{2+} protein) solution (65 μL) (0.5 mg/μmol of protein) to which 21.8 μL of a 118 μm MREd was added (the molar ratio of MTF-zf to MREd is 1:1.1) at room temperature in 40 mM MOPS, pH 7.0, and 0.20 M NaCl. The 12-μL aliquots were withdrawn at 0, 60, 90, 120, and 180 min and added to ice-cold SDS−polyacrylamide gel electrophoresis gel loading buffer, mixed and immediately heated at 75 °C for 5 min, and returned to ice. The digestion products of the time course of proteolysis were then subjected to SDS−PAGE analysis on a 16% SDS−PAGE mini-gel, and then transferred to PVDF membrane for N-terminal sequencing. The digestion product purified by reverse-phase C4 chromatography was characterized by MALDI-TOF.

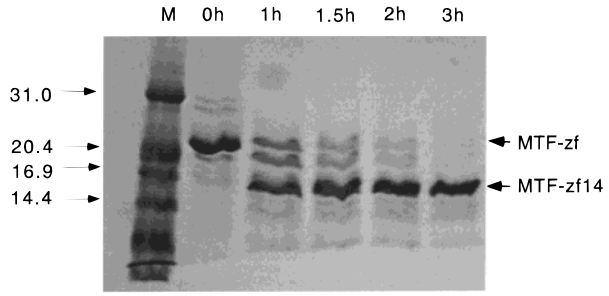

FIGURE 3: SDS−polyacrylamide gel electrophoresis analysis of the time course of trypsinolysis of Zn_6 MTF-zf in the presence of stoichiometric MREd. Conditions: 35 μM MTF-zf; 40 mM MOPS; pH 7.0; 0.20 M NaCl.

RESULTS

The isolated zinc finger domain of human MTF-1, MTF-zf, contains at least two classes of zinc sites which are readily distinguished on the basis of the apparent affinity of each for zinc (*2*). One class of sites contains 3−4 g at mol^{-1} Zn(II) and appears to bind zinc tightly; the zinc in the remaining sites is selectively lost upon dialysis or treatment with a chelator with modest affinity (≈10^7 M^{-1}) for Zn(II) (*2*). In addition, the affinity of complex formation with the MREd appeared to be nearly identical with $Zn_{3.5}$ and Zn_6 MTF-zf proteins and far-UV-CD spectra suggest similar structural contents in both forms of MTF-zf, apparently enough to fold just three or four of six zinc fingers of MTF-zf into typical $\beta\beta\alpha$ units (*2*). This suggested to us that 3−4 of the zinc fingers of MTF-zf play a structural role in folding and high affinity DNA binding. Experiments were therefore designed here to determine which zinc finger domains of the molecule correspond to each class of sites.

Limited Trypsinolysis Experiments. To obtain this information, Zn_6 MTF-zf was subjected to limited proteolysis with trypsin in the presence and absence of a stoichiometric concentration of MREd, and the digestion products were analyzed by denaturing SDS−PAGE (Figure 3). In the absence of DNA, MTF-zf was converted to a mixture of products, with a fragment containing approximately three zinc finger domains a somewhat overrepresented intermediate observed during the time course of proteolysis (data not shown). In contrast, in the presence of the MREd, the MTF-zf is cleanly converted to a fragment with a molecular weight of ≈15 kD which is highly resistant to further proteolysis. There are no other proteolytic fragments of lower molecular weight apparent even after 3 h of trypsin incubation. This DNA-protected digestion product was purified and characterized by amino acid analysis, N-terminal sequencing to give N-Val^{137}-Lys-Tyr-Gln-X, and TOF-MALDI mass spectrometry which returns a M_r = 14455.8. This characterization establishes this protected fragment as containing residues 137−260 (expected M_r = 14443.4) with a major site of tryptic cleavage following Arg^{260}, just C-terminal to the canonical TGEKPF linker connecting fingers 4 and 5 (cf.

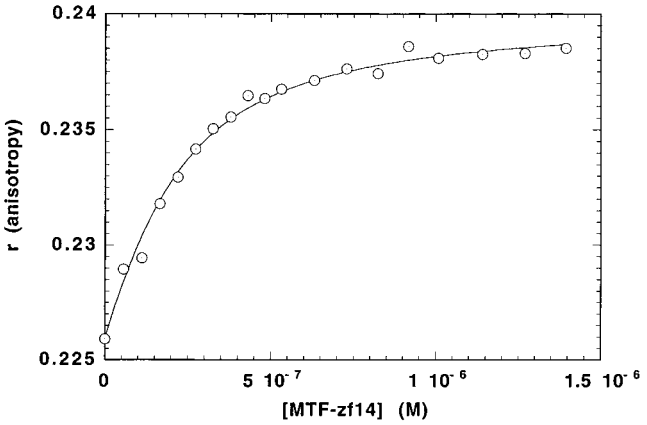

FIGURE 4: MTF-zf14 binds to a coumarin-labeled oligonucleotide duplex containing a single MREd binding site (MREd:2*) consistent with the formation of a 1:1 complex. Conditions: 1.6×10^{-7} M duplex; 40 mM MOPS; 0.20 M NaCl; pH 7.0; 25 °C. The solid line defines a fit to a 1:1 binding model with $K_{app} = 7.9 \times 10^6$ M^{-1}.

Figure 1). Similar results were obtained with Zn_6 and $Zn_{3.5}$ forms of MTF-zf-MREd complex (data not shown).

Characterization and MRE-Binding Activity of MTF-zf14, MTF-zf13, H279N-MTF-zf, and H309N-MTF-zf. The results of trypsinolysis experiments show that the N-terminal four zinc fingers of MTF-zf are resistant to proteolysis upon binding to MREd, with finger domains five and six less so. We next carried out experiments to address the relative importance of fingers 4−6 in stabilizing the MTF-zf-MRE complex. Broken-finger (*44*) and missing-finger (finger deletion) mutants of MTF-zf were prepared and characterized. Deletion mutants MTF-zf13 and MTF-zf14 contain only the N-terminal three and four zinc fingers, respectively, with a C-terminal Trp engineered into each mutant (see Figure 1). MTF-zf14 is nearly identical to the protected fragment generated by limited proteolysis of the MTF-zf:MRE complex (Figure 3), with the polypeptide chain one residue shorter (corresponding to residues 137−259) and containing a $Phe^{259} \rightarrow Trp^{259}$ substitution to facilitate FRET studies (Figure 1). MTF-zf46 contains the three C-terminal zinc fingers. The two broken finger mutants are H279N MTF-zf, which changes the first liganding histidine in finger five, His^{279}, to a nonliganding (*39*) asparagine (MTF-Δzf5), and H309N MTF-zf, which introduces the same substitution in zinc finger 6 (MTF-Δzf6) (Figure 1).

The extent to which various MTF-zfs bind to a 23 base pair coumarin-labeled oligonucleotide duplex harboring a single MREd consensus sequence (MREd:2*; cf. Figure 2) was determined using a fluorescence anisotropy assay. A representative MREd:2* binding isotherm obtained for MTF-zf14 at 0.20 M NaCl, 25 °C, pH 7.0, is shown in Figure 4, with the solid curve the results of a nonlinear least-squares fit to a 1:1 binding model. Under these solution conditions, $K_{app} = 8.8\ (\pm 4.0) \times 10^6\ M^{-1}$ (Table 1), or about 40-fold weaker than that for intact MTF-zf. Analogous experiments carried out with the MTF-zf13 reveal a larger decrease in binding affinity by ≈700-fold (Table 1). Interestingly, the binding affinities determined for H279N-MTF-zf and H309N-MTF-zf to the MREd are quite similar to that obtained for partially oxidized $Zn_{(3)}Cys_6$MTF-zf, in which most of the weak binding finger cysteines are oxidized (*2*). Analytical data show that over the course of the DNA binding experiment, which is carried out in air in the absence of reducing agent, the Cys in this protein become partially oxidized, consistent with the binding affinities observed (data not shown).

To probe the DNA binding specificity of these interactions, two additional oligonucleotides were employed. One is MUT1 DNA, which contains four base pair substitutions on the 3′ or CG-rich side of oligonucleotide, three of which reside within the consensus sequence (cf. Figure 2). A promoter element containing four tandemly arranged MUT1 sequences has been previously shown to be largely inactive in metalloregulation in vivo and fails to band-shift MTF-1 present in crude nuclear extracts (*16*). The other oligonucleotide is MUT2, which contains six base pair substitutions on the 5′ or TGCAC side of oligonucleotide (*32*). As can be seen in Table 1, deletion or mutagenesis of fingers 5 and 6 not only has a large effect on the binding affinity of MTF-zf to the wild-type MREd sequence but appears to have a significant effect on the specificity of the interaction, with MTF-zf13 having lost much of its ability to differentiate among functional and nonfunctional MRE molecules. Isolated Zn_3 MTF-zf46 exhibits no detectable affinity for the MREd under these conditions, consistent with the N-terminal fingers playing a major role in DNA binding (Table 1).

Far-UV-CD Spectra of MTF-zf Derivatives. Previous far-UV-CD spectra obtained for intact MTF-zf were found to be nearly indistinguishable for the $Zn_{5.5}$, $Zn_{3.5}$, and partially oxidized forms of the protein (*2*). Far-UV-CD spectra of intact Zn_6 MTF-zf are shown compared to that of missing finger mutants, MTF-zf14, MTF-zf13, and MTF-zf46, in Figure 5A. Both MTF-zf14 and MTF-zf13 finger deletion molecules are characterized by similar spectra, each of which shows significantly more negative ellipticity per residue than that of MTF-zf, which itself is identical to previously published spectra (*2*). In contrast, MTF-zf46 contains the smallest amount of negative ellipticity. Strikingly, summing the spectra of Zn_3 MTF-zf13 and Zn_3 MTF-zf46 largely recapitulates the spectrum of the entire Zn_6 MTF-zf domain (Figure 5B). This confirms the structural independence of each three finger fragment within the intact zinc finger domain. The structural origin of these spectroscopic differences are unknown; however, one possible explanation is that the N-terminal 3 and 4 fingers are folded into $\beta\beta\alpha$-structures, while the C-terminal fingers 5 and 6 adopt partially folded or non-$\beta\beta\alpha$ structures.[2] Far-UV-CD spectra

[2] A quantitative analysis of the far-UV-CD spectra was carried out using the SELCON3 algorithm and data extending to 180 nm (*1*). In all cases, the root-mean-square (rmsd) difference in the calculated and experimental spectra was slightly above optimal, but qualitative trends in the data do emerge (data not shown). For MTF-zf13 (rmsd = 0.50) and MTF-zf14 (rmsd = 0.77), the converged fits were internally consistent with one another with ≈29% α-helix (regular and distorted), ≈17% β-strand (regular and distorted), ≈22% β-turn, and 28% unordered structure. These fits give 3 (3 expected) and 4 (4 expected) α-helical segments of ≈10 residues in length and 4 (6 expected) and 5 (8 expected) β-strand segments of ≈5 residues in length, for MTF-zf13 and MTFzf14, respectively. These data are largely consistent with 3 and 4 typical $\beta\beta\alpha$-units, respectively, in MTF-zf13 and MTF-zf14. Zn_6 MTF-zf spectra analyzed over the same wavelength range gave (rmsd = 0.68) ≈15% α-helix (regular and distorted), ≈43% β-strand (regular and distorted), ≈23% β-turn, and 22% unordered structure. These fits give 4 α-helical segments of ≈12 residues in length and 12 β-strand segments of an average length of 11 residues. This fit is qualitatively consistent with about 4 $\beta\beta\alpha$ units with the remainder of the molecule (the C-terminal finger domains) adopting nonnative β or other structure.

Table 1: Summary of DNA-Binding Affinities (K_{app}, M^{-1}) of Missing- and Broken-Finger Mutants of MTF-zf to Various Coumarin-Labeled Oligonucleotides[a]

protein	MREd:2*	fold decrease in K_{app} relative to MTF−zf	MUT1	fold decrease in MUT1 K_{app} relative to MREd:2*	MUT2	fold decrease in MUT2 K_{app} relative to MREd:2*
Zn_6 MTF-zf	$3.8(\pm0.5) \times 10^8$	1	$2.2(\pm0.3) \times 10^7$	17	$8.3(\pm1.7) \times 10^6$	46
MTF-zf14	$8.8(\pm4.0) \times 10^6$	43	$4.2(\pm0.5) \times 10^6$	2	$2.9(\pm0.2) \times 10^6$	3
MTF-zf13	$5.2(\pm2.0) \times 10^5$	730	$1.1(\pm0.1) \times 10^6$	0.5	$2.4(\pm0.3) \times 10^5$	2
MTF-zf46[b]	$\leq 10^4$	$\geq 10\,000$				
MTF-Δzf5	$1.4(\pm0.3) \times 10^7$	27				
MTF-Δzf6	$1.1(\pm0.4) \times 10^7$	35				
$Zn_{(3)}Cys_6$ MTF-zf[c]	$1.2(\pm0.2) \times 10^7$	32				

[a] The oligonucleotide sequences are shown in Figure 2. Conditions: 40 mM MOPS; 0.20 M NaCl; pH 7.0; 25 °C. [b] No complex formation could be detected up to 30 μM added protein at 1.6×10^{-7} M MREd:2*. [c] Reference *2*.

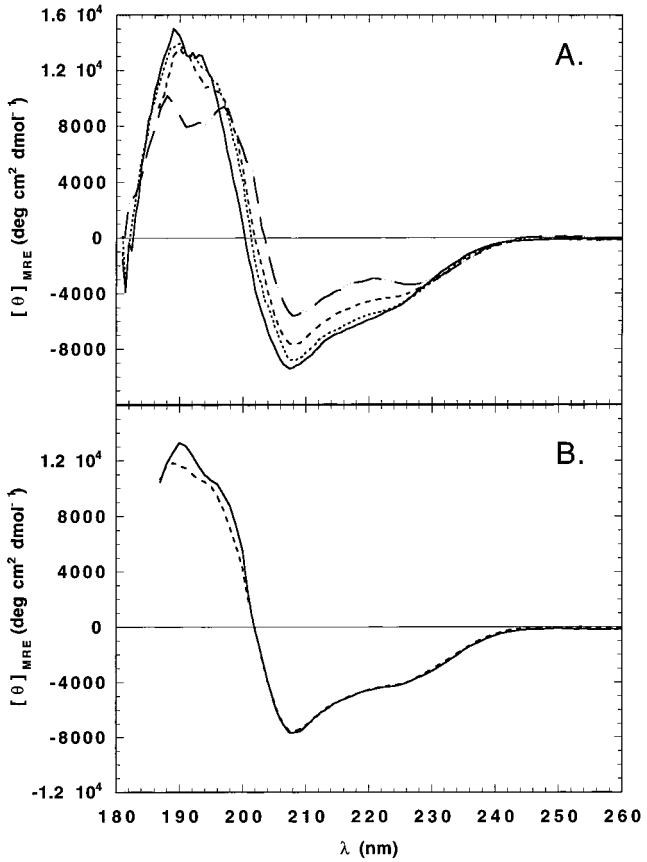

FIGURE 5: (A) Far-UV-CD spectra of various MTFs: MTF-zf (— —); MTF-zf14 (- - -); MTF-zf13 (—); MTF-zf46 (— ··· —). (B) Comparison of the corrected mean residue ellipticity spectrum calculated by summing the MTF-zf13 and MTF-zf46 spectra (- - -) and scaling to 184 residues with that of intact MTF-zf (—). Conditions: 6 mM sodium phosphate; 0.20 M NaF; pH 7.0; 25 °C.

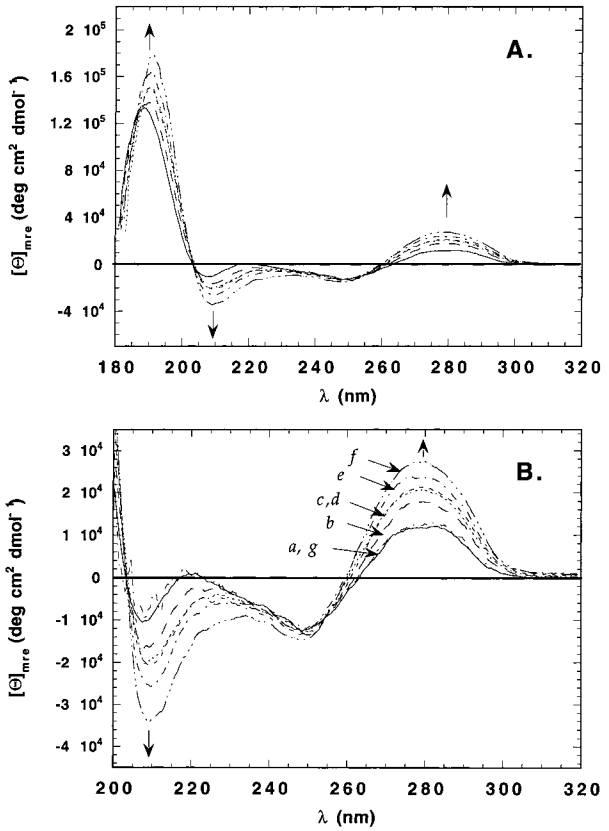

FIGURE 6: UV-CD spectra of the MREd (—, *a*) and difference CD spectra of saturated complexes formed with MTF-zf13 (— —, *b*), MTF-zf14 (- - -, *c*), H279N MTF-zf (···, *d*), H309N MTF-zf (— · —, *e*), and MTF-zf (— ··· —, *f*). Saturated amounts of proteins were added based on K_{app} (Table 1), and the spectral contribution of the free proteins was subtracted. (A) Full spectra from 180 to 320 nm. (B) Enlargement of the spectral changes from 200 to 320 nm. The difference CD spectrum of a 4:1 mixture of a MTF-zf46: MREd complex is also shown here (···, *g*). Conditions: 6 mM sodium phosphate; 0.20 M NaF; pH 7.0; 25 °C. The mean residue ellipticity ($[\Theta]_{MRE}$) is expressed per mole of nucleotide.

of MTF-zf broken finger mutants show that these mutants have approximately the same folded structure as wild-type MTF-zf, as expected (data not shown).

UV-CD Spectra of MTF-zf-MREd Complexes. UV-CD experiments were next carried out to determine if binding to the MREd altered the conformation of the protein, for example, by inducing additional folded structure into the molecule. Surprisingly, it is the conformation of MREd, not MTF-zf, that is changed upon the formation of MTF-MREd complexes. Figure 6 shows the UV-CD spectra of the MREd (pH 7.0, 0.20 M NaF) in its uncomplexed form and spectra obtained with various MTF-zf-MREd complexes. The complex spectra are shown in such a way that the contribution of the free protein has been subtracted, assuming that the free and bound proteins have the same CD spectrum. The concentration of MTF-zf proteins present in each case is up to 5-fold greater than the MREd concentration, ensuring that all the DNA is complexed with protein in each case. The spectrum of the uncomplexed MREd consists of two positive bands at about 280 nm ($\approx$+12 000 deg cm^2 dmol^{-1}) and 190 nm ($\approx$13 400 deg cm^2 dmol^{-1}), two negative bands at about 248 nm ($\approx$−13 000 deg cm^2 dmol^{-1}) and 208 nm ($\approx$−12 000 deg cm^2 dmol^{-1}), and an inflection point at

approximately 260 nm. The intensity at 248 nm is only slightly greater than that at 280 nm. This is a roughly conservative CD spectrum completely consistent with a B-form structure (*45*). Strikingly, the difference spectra obtained for the individual MTF-zf-MREd complexes all show marked increases in the ellipticity at 280, 210, and 190 nm (with no change in the sign), to various degrees depending on the identity of the bound protein. Furthermore, the maximal extent of change obtained with each MTF-zf derivative roughly correlates with binding affinity and is as follows: MTF-zf13 < MTF-zf14 ≈ H279N MTF-zf < H309N MTF-zf < MTF-zf. MTF-zf46 does not induce a conformational change into the MREd (Figure 6B), even at a 4-fold excess of protein to DNA, consistent with the fact that this protein does not bind to the MREd (Table 1). These spectral features are largely as expected for a global change in the MREd to a structure that is more A-like or that which possesses distinct A-like properties that CD is most sensitive (*45*, *46*) (see Discussion). Although a small change in the conformation of individual MTF-zf proteins upon MREd binding cannot be ruled out by these spectra, they seem unlikely since changes in the protein would not give the observed correlation with characteristic nucleic acid bands over the entire 180−320 nm spectral window. This is particularly so in the near-UV region, where it is not possible to attribute these spectral changes to the protein.

Fluorescence Resonance Energy Transfer Spectroscopy. Because coumarin and tryptophan form a good donor−acceptor pair, the interaction between protein and DNA can be monitored by measuring fluorescence energy transfer between the coumarin moiety at either end of the MREd and the single tryptophan residue engineered into the C-terminal end of individual MTF-zf proteins (*41*). This experiment provides information on the distance between donor and acceptor and thus globally defining the topology of the multifinger MTF-zf on the MREd. Figure 7A shows emission spectra of MREd:2* samples excited at 295 nm in the presence of absence of saturating MTF-zf. As can be seen, the binding of MTF-zf leads to an increase in the fluorescence intensity of the coumarin moiety, to a maximal extent of ≈32% in this experiment. This corresponds to a rather high energy transfer efficiency (E = 0.74) (Table 2).

When the same experiment is carried out with MTF-zf14 in place of intact MTF-zf (Figure 7B), two changes occur. First, the overall binding affinity drops by about 50-fold, to a $K_{app} = 4.8 \times 10^6$ M^{-1} from 2.0×10^8 M^{-1} for MTF-zf, consistent with fluorescence anisotropy experiments (Table 1). More importantly, the binding of MTF-zf14 to MREd:2* results in only a 16% increase of fluorescence intensity at 478 nm when excited at 295 nm, or $E = 0.29$. When MTF-zf binds to the MREd:1* oligonucleotide, which is characterized by the same DNA sequence as MREd:2* but with the coumarin moiety on the opposite (5′) side of the core sequence (Figure 2), the fluorescence intensity actually falls slightly ($F_{ad}/F_a = 0.93$) to an extent near that which occurs upon direct excitation of the coumarin−DNA itself ($Q_{ad}/Q_a = 0.91$) (Table 2) (spectral scans not shown) despite their identical binding affinities (*2*). This is consistent with a low energy transfer efficiency for this donor−acceptor pair ($E = 0.09$) (Table 2). The qualitative conclusion from these experiments is that the C-terminal Trp in zinc finger domain 6 is far closer to the GCC side of the consensus sequence, 3′ to the core TGCA core site, and far removed from the opposite end of the oligonucleotide. Moving this Trp just C-terminal to zinc finger 4 moves the coumarin probe on the 3′ side of the core sequence further removed from the new C-terminal Trp residue. This qualitative conclusion is supported by a quantitative analysis of these spectral data, in the which the distance difference between the two Trp−coumarin pairs is ≈15 Å or 5 or so base pairs (Table 2).

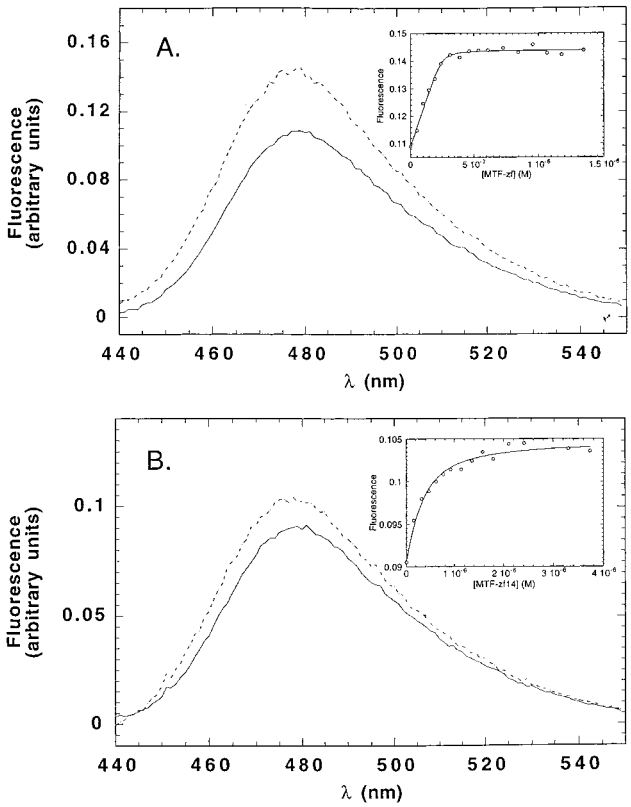

FIGURE 7: Sensitized fluorescence emission spectra of MREd:2* (λ_{ex} = 295 nm) collected in the absence (—) and presence (- - -) of saturating concentrations of MTF-zf (A) or MTF-zf14 (B). Inset: Binding isotherms of MREd:2* with MTF-zf (A) and MTF-zf14 (B) as monitored by an enhancement of DNA fluorescence emission intensity due to FRET from the C-terminal Trp residue in each protein. The continuous curves drawn through the data are fits to a 1:1 binding model: (A) MTF-zf, $K_{app} = 2.0 \times 10^8$ M^{-1}, F_{max} = 0.144; (B) MTF-zf14, $K_{app} = 4.8 \times 10^6$ M^{-1}, F_{max} = 0.105. Conditions: 2.5×10^{-7} M DNA; 40 mM MOPS; pH 7.0; 0.20 M NaCl; 25 °C.

DISCUSSION

The zinc finger transcription factor MTF-1 has been shown to play an essential role in induction of metallothionein gene expression in response to heavy metals in human and mouse cells (*16*, *47*) and is probably identical to other factors previously identified from rat and human liver nuclei (*48*, *49*). To obtain molecular insight into MTF-1 function, we have subcloned, overexpressed, and purified (*2*) the zinc finger domain (MTF-zf) of human MTF-1 (*28*). Purified MTF-zf binds to the metal responsive element with high affinity and specificity. In previous work, we detected at least two classes of zinc finger domains in MTF-zf (*2*). One class of sites containing 3 to 4 zinc fingers has zinc binding and DNA binding properties consistent with a structural role, while the other group of zinc finger sites is characterized by

Table 2: Fluorescence Resonance Energy Transfer Parameters for Various MTF-zf-MREd Complexes[a]

parameter	MTF-zf-MREd:2*	MTF-zf-MREd:1*	MTF-zf14-MREd:2*
Q_a/Q_{ad}[b]	0.93 ± 0.08	1.10 ± 0.04	0.93 ± 0.04
F_{ad}/F_a[c]	1.35 ± 0.03	0.93 ± 0.02	1.16 ± 0.02
E[d]	0.74 ± 0.03	0.09 ± 0.02	0.29 ± 0.03
J (M^{-1} cm^3)	4.47×10^{-14}	2.83×10^{-14}	4.46×10^{-14}
Q_d[e]	0.144	0.144	0.276
r_d	0.051	0.051	0.042
τ_d (ns)[f]	3.3 (2.8)	3.3 (2.8)	5.3 (1.0)
R_o (Å)[g]	31.5	29.2	35.1
R (Å)[h]	26	43± 2	41
R (Å), with range in κ^2 from r_d, r_a[i]	23−32	38−51	37−48

[a] Determined using data like those shown in Figure 7. [b] Determined from steady-state anisotropy experiments as described (*2*). ($\lambda_{ex} = 430$ nm). [c] Determined at $\lambda_{em} = 478$ nm from at least two independent experiments. [d] From eq 1. [e] Determined from $Q = 0.140$ for *N*-acetyltryptophanamide (NATA). [f] Determined using a model which incorporates one discrete (<5% of the signal in each case) and one Lorentzian component (>95% of the signal) with the center and width (in parentheses) of the Lorentzian distribution given. NATA is characterized by a single discrete lifetime of 2.8 ns under these conditions. [g] From eq 3. [h] From eq 2. [i] See ref *43*.

properties consistent with a metalloregulatory role (a weak apparent zinc-binding affinity).

Metal Site Heterogeneity and MTF-zf Folding. We showed previously that MTF-zf as isolated contains as little as 3 and as many as 6 molar equiv of bound zinc under conditions where all 12 Cys in the molecule are reduced and theoretically competent to bind metals, predicted to form $\beta\beta\alpha$ structures (*2*). The same behavior is true of an N-terminally extended version of MTF-zf containing residues 113−320 (data not shown). The far-UV−CD spectra, reflective of secondary structure content, of each of these MTF-zf proteins are identical to one another and nearly indistinguishable from MTF-zf in which the Cys in the weak binding fingers are oxidized, presumably to disulfide bonds. We suggested previously that each of these forms corresponds to a partially folded molecule in which some or all of the weak binding fingers are not folded into $\beta\beta\alpha$ structures, even in the Zn_6 form as isolated (*2*).[2] The evidence we present here conclusively demonstrates that the weak zinc binding fingers in MTF-zf minimally correspond to zinc finger domains 5 and 6. Furthermore, the simplest interpretation of the far-UV-CD spectra is that the structures of finger domains 1−3 and 4−6 may well be different from one another and that these differences are maintained in the isolated three-finger domain fragments (Figure 5). Since the N-terminal four fingers provide a large fraction of the MRE-binding energy (Table 1), it seems reasonable to conclude that fingers 1−4 adopt typical $\beta\beta\alpha$ structures; if this is the case, the C-terminal finger domains may adopt a non-$\beta\beta\alpha$ or partially folded structure (Figure 5).[3] This may be the structural basis of their lower apparent affinity for metal ions. Preliminary Co(II)-substitution experiments show that all six fingers in MTF-zf are capable of forming tetrahedral Co(II) complexes (X.C. and D.P.G., unpublished results).

Metal Site Heterogeneity and Specific MREd Binding. Limited trypsinolysis of MTF-zf in the presence of MREd results in the formation of a trypsin-resistant core fragment encompassing the N-terminal four zinc fingers, while C-terminal finger domains 5 and 6 are completely digested into smaller fragments. Thus, the weak zinc binding finger domains of MTF-zf are also bound to the MREd in a conformation distinct from that of zinc fingers 1−4, which must be intimately bound to the DNA, at least as measured by limited proteolysis. Broken-finger mutants H279N MTF-zf (MTF-Δzf5) and H309N MTF-zf (MTF-Δzf6) and deletion mutants MTF-zf14 and MTF-zf13 were therefore purified and characterized to determine the energetic contribution that these domains make to MREd binding. Broken-finger mutants Δzf5 and Δzf6 and the missing-finger mutant MTF-zf14 all have comparable affinities for the MREd, reduced ≈25−40-fold relative to MTF-zf; deletion of finger 4 results in further ≈20-fold reduction in MREd binding affinity and a significant loss in DNA binding specificity. Thus, the N-terminal four fingers in MTF-zf are minimally required for high-affinity MREd binding. However, deletion of the weak zinc binding C-terminal fingers is clearly destabilizing which suggests that all six zinc finger sequences are necessary for stable and specific DNA complex formation by MTF-zf to a single MREd.

MREd Conformational Changes upon MTF-zf Binding. The UV-circular dichroism spectra of the free MREd oligonucleotide compared to difference spectra of MREd-MTF-zf complexes provide additional structural insight into the participation of C-terminal zinc finger sequences in stable complex formation. The UV-CD spectrum of the MREd reveals that the MREd adopts a typical B-form structure. However, binding of MTF-zf results in a dramatic change in the spectrum, which cannot be attributed to protein structural changes. The specific increases in CD band intensity induced by MTF-zf binding are generally similar to the published spectra of A-like duplexes (*52*); in particular, the pronounced increase in the negative ellipticity band at 210 nm is significant in the basis spectra that characterize the CD of nucleic acid hybrids and is due almost entirely to base pairing in A-form structures (*46*). At least part of the pronounced effect on MREd structure could be due to the dehydration of the lattice since incubation of B-form nucleic acid polymers with dehydrating agents including ethanol and trifluoroethanol are known to efficiently induce A-form structure (*45*). Preliminary experiments suggest that 80% trifluoroethanol induces conformational changes in the MREd duplex that are distinct but globally similar to those induced by the binding of MTF-zf (data not shown). This is consistent with our interpretation of the thermodynamics of MREd-MTF-zf complex formation, which suggest that binding is

[3] Preliminary $^1H-^{15}N$ HSQC NMR experiments clearly show that Zn(II) binding induces folded structure into MTF-zf46 (X.C. and D.P.G., unpublished results).

accompanied by significant burial of hydrophobic surface area and release of bound water molecules (*2*).

It is widely known that Cys_2-His_2 zinc finger proteins are capable of binding to double-stranded RNA sequences (*53*−*58*) as well as RNA−DNA hybrids (*59*), which presumably adopt A-like helical structures. Previous CD studies of TFIIIA internal control region (ICR) revealed that the DNA is largely B-form but has definite features characteristic of A-form structure (*60*). The conformation of the ICR does not change upon TFIIIA binding as measured by CD (*60*), in strong contrast to the results shown here; the NMR (*61*) and crystallographic (*62*) structures of two truncated TFIIIA-5S rDNA complexes however reveal that the DNA is essentially B-form. In contrast, the DNA in another complex of a Cys_2-His_2 zinc finger protein (mouse GLI) with DNA (*63*) reveals that the bound DNA adopts a conformation that can be described as possessing structure features characteristic of both canonical A- and B-form families (*64*). This has been termed the B_{eg} or an "enlarged-groove" B-form conformation. A similar DNA conformation was also observed in the high-resolution crystal structure of the Zif268−DNA complex (*64*). Although CD studies of the GLI−DNA complex have not been reported, a CD spectrum of the Zif268−DNA complex in the 220−320 nm region is qualitatively similar to those reported here (*64*). The structural features to which near-UV-CD spectroscopy may be most sensitive, base stacking, are A-like features in the B_{eg} conformation (*65*). For example, B_{eg} is characterized by a widening of the major (and minor) grooves which results in an increase in the helical diameter; this displaces the base pairs toward the outside of the helix and makes them significantly inclined relative to the helical axis (*65*). Both of these features are characteristic of A-form duplexes. What sequence determinants in MTF-zf drive this conformational transition in the MREd are unknown; however, modeling studies suggest that the short, nearly canonical linker lengths in MTF-zf may be at least partly responsible for this (*64*). Interestingly, a Thr-Trp-Thr triplet in the −1-+1-+2 positions relative to the start of the α-helix in TFIIIA and a related Xenopus protein 5S RNA binding protein p43 (*55, 59*) appears to play a significant role in specific *RNA* binding; interesting, structural zinc fingers 3 and 4 in MTF-zf are predicted to have conservatively substituted Thr-Leu-Tyr and Thr-Leu-Ser triplets in an analogous position.

Strikingly, we find a very good correlation between the maximal extent of structural transition induced by the binding of mutant MTF-zf proteins and relative binding affinity. MTF-zf induces the maximal structural change into the MREd, and the broken finger mutant Δzf6 is next, while Δzf5 induces a comparatively lesser change which is comparable to MTF-zf14. The smallest extent of structural transition is induced by MTF-zf13, which binds the weakest of any MTF-zf derivative. These findings suggest a nucleation−propagation model for the structural transition in the MREd, in which weak zinc binding finger sequences 5 and 6 significantly modulate MREd binding affinity by propagating B_{eg}-like structural features in the oligonucleotide nucleated by one or more of the N-terminal fingers. Consistent with this idea is the finding that MTF-zf46 does not alter the conformation of the MREd. We suggest that both fingers 5 and 6 contact the DNA in a way which is distinct from that of fingers 1−4 but appear essential for properly positioning MTF-zf on the oligonucleotide in order to enable high affinity and specificity of binding. Distinct structural dispositions of individual zinc fingers when bound to a specific DNA target are not unique to MTF-zf, having been found to occur crystallographically in both the five-finger GLI (*63*) and six-finger TFIIIA DNA complexes. These structural findings, however, suggest the possibility that a local conformational change may in some way be involved in zinc metalloregulation in this system. At least one previous report provides some evidence of a conformational change in the DNA as evidenced by DNAse I hypersensitivity in a region of the DNA between two oppositely oriented MRE binding sites in the MT-IIA promoter (*49*).

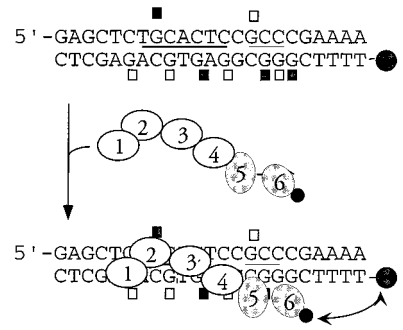

FIGURE 8: Cartoon model of the interaction of MTF-zf with the MREd oligonucleotide derived from the studies presented here. The C-terminal Trp energy transfer donor and the coumarin acceptor are indicated by the small and large filled circles, respectively. The filled and open boxes represent N7 atoms of guanine residues which when methylated inhibit MTF-1-MREd complex formation to strong and weak degrees, respectively (*51*). The DNA also undergoes a marked conformational change (from canonical B to A- or B_{eg}-like) on binding MTF-zf not illustrated here. Weak Zn(II) binding and DNA zinc fingers 5 and 6 are shaded to differentiate them from N-terminal fingers 1−4. The model is only meant to illustrate global features of the complex.

Global Orientation of the MTF-zf on the MREd. Fluorescence resonance energy transfer from a donor to an acceptor is one of the most extensively used methods used to study macromolecular distances in solution (*66*). The spectral overlap of the emission spectrum of a donor with the absorption spectrum of an acceptor is a required condition for the fluorescence resonance energy transfer to occur. In our case, there is significant spectral overlap of the tryptophan emission with the coumarin absorption spectrum (spectra not shown), indicating that efficient fluorescence energy transfer can occur, provided the tryptophan residue in protein and coumarin in the DNA are in close proximity. The R_o for this donor−acceptor pair is ≈30−35 Å depending on the complex (Table 2). Although three donor−acceptor distances are obviously not sufficient to define the structure of the complex in detail, they unambiguously define the global orientation of this multifinger protein on the MREd in a way which is consistent with the cartoon of the complex shown in Figure 8. On the basis of our steady-state fluorescence measurements, the C-terminus of zinc finger 6 is ≈25 Å from the downstream side of MREd and ≥43 Å from the upstream side containing the core sequence; this places finger 6 (and presumably finger 5) closest to the GCC end of the consensus site. If one makes the assumption that the C-terminus of zinc finger 4 is similarly positioned in the MTF-zf and MTF-zf14 complexes, then this would place finger 4 closest to the TGCAC core sequence. We therefore suggest that the

N-terminal structural fingers associate most intimately with the highly conserved TGCAC core of the metal-response element.

In summary, the N-terminal four zinc fingers of MTF-zf have higher apparent affinity for Zn(II) as well as for MREd; these fingers bind to the MREd on the TGCAC side in a conformation that is relatively resistant to trypsinolysis. The C-terminal zinc fingers 5 and 6 have a lower apparent affinity for Zn(II) and possess a low intrinsic affinity for the MREd; these finger domains interact with the C-rich side of MREd in a way which is distinct from that of zinc fingers 1−4. The precise conformations adopted by any of the finger domains, in particular finger domains 5 and 6, is not yet known with certainty; however, all six zinc fingers clearly contribute to the overall capacity of MTF-1 zinc finger fragment to form stable and specific complexes with the MREd. These results suggest that the N-terminal zinc fingers in MTF-zf are required for high affinity and specific binding to the consensus TGCRCnC core in a way which is subjected to structural and allosteric modulation by the weak zinc binding C-terminal zinc fingers.

The significance of these findings for the mechanism of metalloregulation by MTF-1 is unknown, principally because it is not yet been determined if properties of the isolated zinc finger fragment extend to intact MTF-1. If they do, they certainly suggest that the C-terminal finger domains could play an important role in metalloregulation by modulating the specificity and affinity of MTF-1 for the MRE. Consistent with this, numerous reports have shown that the in vitro binding of full-length MTF-1 to the MRE sequences as analyzed by band-shift analysis, covalent cross-linking, or footprinting analysis, in either partially purified form or in crude extracts, can be reversibly activated by added zinc usually in the 10−100 μM concentration range (*16*, *32*, *36*, *50*, *51*, *53*). Although the zinc content of MTF-1 in these preparations, and whether it is different before and after zinc treatment, has not yet been determined, our studies suggest that this modulation may occur through reversible zinc occupancy of the C-terminal fingers. Other possibilities exist however. The N-terminal finger domains could be metalloregulatory since folding of these domains into $\beta\beta\alpha$-structures is obviously required for MRE binding. This seems unlikely to us given the high apparent affinity of these fingers for zinc (*2*). However, it is possible that domains immediately adjacent to the zinc finger domain and not present in MTF-zf, e.g., the N-terminal region and transcriptional activation domains, significantly alter the metal and DNA properties of MTF-1 via other levels of intramolecular allostery, like that previously observed in the *S. cerevisiae* copper-dependent regulator Mac1 (*67*) and speculated for the yeast zinc-dependent metalloregulatory protein, Zap1 (*68*). Further structural and functional studies will be required to more precisely define the conformation of individual domains of MTF-zf and the mechanism of metalloregulation in this system.

ACKNOWLEDGMENT

We thank the anonymous reviewers for critically reading and offering suggestions for improving the manuscript. We also thank Dr. Greg Reinhart (TAMU) for providing his assistance in determining the fluorescence lifetimes for various MTF-zf derivatives on instrumentation supported by grants from the NIH (GM33216) and the Texas Advanced Research Program.

REFERENCES

1. Sreeraman, N., Venyaminov, S. Y., and Woody, R. W. (1999) *Protein Sci. 8*, 370−380.
2. Chen, X., Agarwal, A., and Giedroc, D. P. (1998) *Biochemistry 37*, 11152−11161.
3. O'Halloran, T. V. (1993) *Science 261*, 715−725.
4. Klausner, R. D., Rouault, T. A., and Harford, J. B. (1993) *Cell 72*, 19−28.
5. Graden, J. A., Posewitz, M. C., Simon, J. R., George, G. N., Pickering, I. J., and Winge, D. R. (1996) *Biochemistry 35*, 14583−14589.
6. Dameron, C. T., George, G. N., Arnold, P., Santhanagopalan, V., and Winge, D. R. (1993) *Biochemistry 32*, 7294−7301.
7. Ansari, A. Z., Bradner, J. E., and O'Halloran, T. V. (1995) *Nature 364*, 371−375.
8. Shi, W., Wu, J., and Rosen, B. P. (1994) *J. Biol. Chem. 269*, 19826−19829.
9. Bsat, N., Herbig, A., Casillas-Martinez, L., Setlow, P., and Helmann, J. D. (1998) *Mol. Microbiol. 29*, 189−198.
10. Gaballa, A., and Helmann, J. D. (1998) *J. Bacteriol. 180*, 5815−5821.
11. Pohl, E., Holmes, R. K., and Hol, W. G. J. (1998) *J. Biol. Chem. 273*, 22420−22427.
12. Ralston, D. M., and O'Halloran, T. V. (1990) *Proc. Natl. Acad. Sci. U.S.A. 87*, 3846−3850.
13. Luchinat, C., and Sola, M. (1994) in *Encyclopedia of Inorganic Chemistry* (King, R. B., Ed.) pp 4406−4434, John Wiley and Sons, Ltd., Sussex, England.
14. Coleman, J. E. (1992) *Annu. Rev. Biochem. 61*, 897−946.
15. Berg, J. M., and Shi, Y. (1996) *Science 271*, 1081−1085.
16. Radtke, F., Heuchel, R., Georgiev, O., Hergersberg, M., Gariglio, M., Dembic, Z., and Schaffner, W. (1993) *EMBO J. 12*, 1355−1362.
17. Grotz, N., Fox, T., Connolly, E., Park, W., Guerinot, M. L., and Eide, D. (1998) *Proc. Natl. Acad. Sci. U.S.A. 95*, 7220−7224.
18. Zhao, H., and Eide, D. (1996) *Proc. Natl. Acad. Sci. U.S.A. 93*, 2454−2458.
19. Patzer, S. I. and Hantke, K. (1998) *Mol. Microbiol. 28*, 1199−1210.
20. Erbe, J. L., Taylor, K. B., and Hall, L. M. (1995) *Nucleic Acids Res. 23*, 2472−2478.
21. Noll, M., Petrukhin, K., and Lutsenko, S. (1998) *J. Biol. Chem. 273*, 21393-21401.
22. Morby, A. P., Turner, J. S., Huckle, J. W., and Robinson, N. J. (1993) *Nucleic Acids Res. 21*, 921−925.
23. Thelwell, C., Robinson, N. J., and Turner-Cavet, J. S. (1998) *Proc. Natl. Acad. Sci. U.S.A. 95*, 10728−10733.
24. Escolar, L., Pérez-Martín, J., and de Lorenzo, V. (1998) *J. Mol. Biol. 283*, 537−547.
25. Turner, J. S., Glands, P. D., Samson, A. C. R., and Robinson, N. J. (1996) *Nucleic Acids Res. 19*, 3714−3721.
26. Zhao, H., and Eide, D. J. (1997) *Mol. Cell. Biol. 17*, 5044−5052.
27. Stuart, G. W., Searle, P. F., and Palmiter, R. D. (1985) *Nature 317*, 828−831.
28. Brugnera, E., Georgiev, O., Radtke, F., Heuchel, R., Baker, E., Sutherland, G. R., and Schaffner, W. (1994) *Nucleic Acids Res. 22*, 3167−3173.
29. Heuchel, R., Radtke, F., Georgiev, O., Stark, G., Aguet, M., and Schaffner, W. (1994) *EMBO J. 13*, 2870−2875.
30. Stuart, G. W., Searle, P. F., Chen, H. Y., Brinster, R. L., and Palmiter, R. D. (1984) *Proc. Natl. Acad. Sci. U.S.A. 81*, 7318−7322.
31. Párraga, G., Horvath, S. J., Eisen, A., Taylor, W. E., Hood, L., Young, E. T., and Klevit, R. E. (1988) *Science 241*, 1489−1492.
32. Dalton, T. P., Bittel, D., and Andrews, G. K. (1997) *Mol. Cell. Biol. 17*, 2781−2789.

33. Günes, C., Heuchel, R., Georgiev, O., Müller, K.-H., Lichtlen, P., Blüthmann, H., Marino, S., Aguzzi, A., and Schaffner, W. (1998) *EMBO J. 17*, 2846−2854.
34. Dalton, T. P., Li, Q., Bittel, D., Liang, L., and Andrews, G. K. (1996) *J. Biol. Chem. 271*, 25233−25241.
35. Dalton, T., Palmiter, R. D., and Andrews, G. K. (1994) *Nucleic Acids Res. 22*, 5016−5023.
36. Bittel, D., Dalton, T., Samson, S. L. A., Gedamu, L., and Andrews, G. K. (1998) *J. Biol. Chem. 273*, 7127−7133.
37. Li, Q., Hu, N., Daggett, M. A. F., Chu, W. A., Bittel, D., Johnson, J. A., and Andrews, G. K. (1998) *Nucleic Acids Res. 26*, 5182−5189.
38. Chu, W. A., Moehlenkamp, J. D., Bittel, D., Andrews, G. K., and Johnson, J. A. (1999) *J. Biol. Chem. 274*, 5279−5284.
39. Guo, J., and Giedroc, D. P. (1997) *Biochemistry 36*, 730−742.
40. Del Rio, S., and Setzer, D. R. (1993) *Proc. Natl. Acad. Sci. U.S.A. 90*, 168−172.
41. Heyduk, T., and Lee, J. C. (1990) *Proc. Natl. Acad. Sci. U.S.A. 87*, 1744−1748.
42. Jezewska, M. J., Rajendran, S., Bujalowska, D., and Bujalowski, W. (1998) *J. Biol. Chem. 273*, 10515−10529.
43. Giedroc, D. P., Khan, R., and Barnhart, K. (1991) *Biochemistry 30*, 8230−8242.
44. Del Rio, S., Menezes, S. R., and Setzer, D. R. (1993) *J. Mol. Biol. 233*, 567−579.
45. Johnson, W. C., Jr. (1996) in *Circular Dichroism and the Conformational Analysis of Biomolecules*, pp 433−468, Plenum Press, New York.
46. Hashem, G. M., Pham, L., Vaughn, M. R., and Gray, D. M. (1998) *Biochemistry 37*, 61−72.
47. Samson, S. L. A., and Gedamu, L. (1998) *Prog. Nucleic Acid Res. Mol. Biol. 59*, 257−288.
48. Searle, P. F. (1990) *Nucleic Acids Res. 18*, 4683−4690.
49. Otsuka, F., Iwamatsu, A., Suzuki, K., Ohsawa, M., Hamer, D. H., and Koizumi, S. (1994) *J. Biol. Chem. 269*, 23700−23707.
50. Guo, J., Wang, S., Dong, J., Qiu, H., Scott, R. A., and Giedroc, D. P. (1995) *J. Am. Chem. Soc. 117*, 9437−9440.
51. Westin, G., and Schaffner, W. (1988) *EMBO J. 7*, 3763−3770.
52. Gray, D. M. (1996) in *Circular Dichroism and the Conformational Analysis of Biomolecules*, pp 469−500, Plenum Press, New York.
53. Friesen, W. J., and Darby, M. K. (1997) *J. Biol. Chem. 272*, 10994−10997.
54. Friesen, W. J., and Darby, M. K. (1998) *Nat. Struct. Biol. 5*, 543−546.
55. Clemens, K. R., Wolf, V., McBryant, S. J., Zhang, P., Liao, X., Wright, P. E., and Gottesfeld, J. M. (1993) *Science 260*, 530−533.
56. Köster, M., Kühn, U., Bouwmeester, T., Nietfeld, W., El-Baradi, T., Knöchel, W., and Pieler, T. (1991) *EMBO J. 10*, 3087−3093.
57. Finerty, P. J., Jr., and Bass, B. L. (1997) *J. Mol. Biol. 271*, 195−208.
58. Joho, K. E., Darby, M. K., Crawford, E. T., and Brown, D. D. (1990) *Cell 61*, 293−300.
59. Shi, Y., and Berg, J. M. (1995) *Science 268*, 282−284.
60. Huber, P. W., Blobe, G. C., and Kartmann, K. M. (1991) *J. Biol. Chem. 266*, 3278−3286.
61. Foster, M. P., Wuttke, D. S., Radhakrishnan, I., Case, D. A., Gottesfeld, J. M., and Wright, P. E. (1997) *Nat. Struct. Biol. 4*, 605−608.
62. Nolte, R. T., Conlin, R. M., Harrison, S. C., and Brown, R. S. (1998) *Proc. Natl. Acad. Sci. U.S.A. 95*, 2938−2943.
63. Pavletich, N. P., and Pabo, C. O. (1993) *Science 261*, 1701−1707.
64. Elrod-Erickson, M., Rould, M. A., Nekludova, L., and Pabo, C. O. (1996) *Structure 4*, 171−1180.
65. Nekludova, L., and Pabo, C. O. (1994) *Proc. Natl. Acad. Sci. U.S.A. 91*, 6948−6952.
66. Selvin, P. R. (1995) *Methods Enzymol. 246*, 300−343.
67. Jensen, L. T., and Winge, D. R. (1998) *EMBO J. 17*, 5400−5408.
68. Zhao, H., and Eide, D. J. (1997) *Mol. Cell. Biol. 17*, 5044−5052.

BI9913000